Preventing Dimensional Collapse in Contrastive Local Learning with Subsampling

Louis Fournier [1] **Adeetya Patel** [2] **Michael Eickenberg** [3] **Edouard Oyallon** [1] **Eugene Belilovsky** [2]

Abstract

This paper presents an investigation of the challenges of training Deep Neural Networks (DNNs) via self-supervised objectives, using local learning as a parallelizable alternative to traditional backpropagation. In our approach, DNN are segmented into distinct blocks, each updated independently via gradients provided by small local auxiliary Neural Networks (NNs). Despite the evident computational benefits, extensive splits often result in performance degradation. Through analysis of a synthetic example, we identify a layer-wise dimensional collapse as a major factor behind such performance losses. To counter this, we propose a novel and straightforward sampling strategy based on blockwise feature-similarity, explicitly designed to evade such dimensional collapse.

1. Introduction

Training a DNN via backpropagation is a computationally expensive process, necessitating the sequential and synchronous processing of layers while storing intermediary computations in memory (Jaderberg et al., 2017). A promising alternative is local learning, where a NN is divided into smaller blocks updated in parallel via local gradient estimates from small auxiliary NNs, allowing efficient parallelization of compute and limited memory use. Nonetheless, larger splits in supervised settings often result in a more significant accuracy gap with End-to-End training (Belilovsky et al., 2021) which is often attributed to information loss, where the auxiliary NN may concentrate only on features relevant to its specific task, inadvertently allowing other potentially useful features for subsequent layers to dissipate.

This phenomenon seems also present in unsupervised settings as very deep NNs are usually split in a limited number of blocks (only 4 in Löwe et al. (2019); Siddiqui et al. (2023)), limiting their parallelization potential. In this paper, we consider the challenge of dividing a NN trained via self-supervision into a larger split while maintaining competitive final accuracy. We focus on approaching the contrastive learning SimCLR framework (Chen et al., 2020), a leading contrastive learning method, through the lens of local learning, owing to its simplicity and widespread use.

Our contributions are as follows: **(1)** We identify a dimensional collapse phenomenon caused by local self-supervised learning resulting in an undesirable information loss. **(2)** Motivated by a synthetic experiment, we propose a simple feature-similarity-based sampling method that prevents this collapse in local learning settings, reducing information degradation. **(3)** Our experiments conducted on the CIFAR-10, Fashion-MNIST and STL-10 datasets validate the effectiveness of our method. **(4)** We carry out ablation experiments on the CIFAR-10 dataset to emphasize the improvement achieved through our method, notably over the dimensional collapse.

Our code is available at: `https://github.com/fournierlouis/subsampled_local_simclr`.

2. Related Work

Contrastive self-supervised learning Contrastive methods for self-supervised learning have made significant strides in recent years. They learn representations by contrasting positive (similar) and negative (dissimilar) examples. Notably, MoCo (He et al., 2019) uses a dynamic dictionary to store features, while the SimCLR (Chen et al., 2020) framework on which we focus this work leverages data augmentation strategies to produce positive examples. However, Jing et al. (2022) noted that contrastive training leads to dimensional collapse without proper projectors, a similar phenomenon to the one we find in local learning.

Supervised local learning Local learning methods have been extensively explored (Nøkland & Eidnes, 2019; Belilovsky et al., 2021; 2019; Gomez et al., 2022; Ren et al., 2022) to eliminate computational locks inherent in

[1]Sorbonne Université, CNRS, ISIR, Paris, France [2]MILA, Concordia University, Montréal, Canada [3]CCM, Flatiron Institute, New York, USA. Correspondence to: Louis Fournier <louis.fournier@isir.upmc.fr>.

In *ICML Workshop on Localized Learning (LLW)*, Honolulu, Hawaii, USA. 2023.

backpropagation (Jaderberg et al., 2017). As local losses greedily optimize the supervised loss, they produce suboptimal intermediate representations as shown by Wang et al. (2021). They rectify this with a computationally expensive reconstruction loss, which we do not require.

Self-supervised local learning Löwe et al. (2019) proposed a self-supervised method based on mutual information criteria for predicting patches from the same image, albeit with few splits. Xiong et al. (2020) expanded on this idea but violated the decoupling principle. Illing et al. (2021) also expanded on the idea with a Hebbian learning method, and Siddiqui et al. (2023) proposed the Barlow Twins loss for local decoupled learning on the ImageNet dataset. However, both showed a similar accuracy loss due to decoupling.

Data subsampling methods in self-supervised learning Various data sampling strategies have been proposed to improve training in the SimCLR framework. In particular, hard negative sampling prioritizes challenging negative examples (Robinson et al., 2021), but is mainly designed for metric learning. Some like Tabassum et al. (2022) refine the method with more intricate reweighting schemes. Our method, considering only high feature similarity examples, is related to these approaches; but does not require additional computation for importance scores, and improves specifically local learning.

3. Method

3.1. Framework: Decoupled SimCLR

We adapt the typical SimCLR pipeline to a decoupled NN composed of K blocks, following Belilovsky et al. (2021). Data augmentation is applied to a batch of size N, generating $2N$ augmented data examples. Each pair of data-augmented examples is considered a positive example; and all other possible pairs are considered negative examples. This results in N positive and $2N(N-1)$ negative pairs.

Each block of the decoupled network, a small network f^k, forward-propagates features to the next block f^{k+1} without receiving gradients from it; which gives the intermediate representations $h_i^k = f^k(h_i^{k-1})$ (with the sample $x_i = h_i^0$). Then, the K small projector head networks g^k project the representations to $z_i^k = g^k(h_i^k)$. For unlocking backward and update steps (see Jaderberg et al. (2017)), each pair $\{f^k, g^k\}$ is updated locally via backpropagation following the local loss of the block. With the similarity score $\mathrm{sim}(x_i, x_j)$ (here the cosine similarity) associated with each pair of samples and τ a temperature parameter, this loss is the decoupled SimCLR loss:

$$\ell_{i,j}^k = -\log \frac{\exp(\mathrm{sim}(\boldsymbol{z}_i^k, \boldsymbol{z}_j^k)/\tau)}{\sum_{l=1}^{2N} \mathbb{1}_{l\neq i} \exp(\mathrm{sim}(\boldsymbol{z}_i^k, \boldsymbol{z}_l^k)/\tau)}. \quad (1)$$

This decoupled training procedure, as it stands, is unable to guide the initial blocks to preserve information that could be crucial for the subsequent blocks, as we discuss in Sec. 4.2. We hypothesize that limiting the learning of the decoupled NN to a subsampled set of examples can potentially enhance its convergence behavior by stabilizing the features in the intermediate levels, which we motivate with the following linear model.

3.2. Preventing dimensional collapse in a linear model with subsampling

Linear model framework We consider the framework presented by Jing et al. (2022) which simplifies the contrastive framework by implementing a linear model W. We consider a dataset composed of two views of N data points $(x_i)_i$ and $(x'_i)_i$ of dimension D, x the concatenated dataset vector and $z = Wx$ the representation vector. Then, the dynamic of the weight matrix under gradient descent following the contrastive InfoNCE loss is, with similarity terms $s_{ij} = \frac{1}{Z_i} e^{-\frac{1}{2}|z_i - z_j|^2}$, $s_{ii} = \frac{1}{Z_i} e^{-\frac{1}{2}|z_i - z'_i|^2}$ and $Z_i = \sum_{j\neq i} e^{-\frac{1}{2}|z_i - z_j|^2} + e^{-\frac{1}{2}|z_i - z'_i|^2}$:

$$\frac{d}{dt}W = \underbrace{\sum_{i,j} s_{ij}(z_i - z_j)(x_i - x_j)^T}_{\text{Data distribution term}} - \underbrace{\sum_i (1 - s_{ii})(z'_i - z_i)(x'_i - x_i)^T}_{\text{Data augmentation distribution term}} \quad (2)$$

For fixed values $(s_{ij})_{ij}$, Jing et al. (2022) finds that strong data augmentation results in collapsed dimensions in W due to negative eigenvalues in $\frac{d}{dt}W$ caused by the data augmentation distribution term. Indeed, at convergence, $\frac{d}{dt}W = 0$. For the sake of simplicity, if two data-augmented samples should lead to the same exact representation, one has that $(s_{ii})_i = 1$ and thus $(s_{ij})_i = 0$.

Following Jing et al. (2022), if data augmentation is only applied at certain features $[d+1 : D]$, then the highest rank matrix W which allows convergence is proportional to $\begin{pmatrix} I_d & 0 \\ 0 & 0 \end{pmatrix}$, and the augmented feature dimensions need to be collapsed.

Subsampling to prevent collapse Now, consider that we restrict both sums to only consider examples with high simi-

larity. Then, at equilibrium:

$$\sum_{i,j,z_i \approx z_j} s_{ij}(z_i - z_j)(x_i - x_j)^T - \sum_{i,z_i \approx z'_i} (1 - s_{ii})(z'_i - z_i)(x'_i - x_i)^T = 0 \tag{3}$$

This is less restrictive, as e.g., $W = I_D$ is an equilibrium point, with no need for collapsed dimensions, while preserving the contrastive nature of the loss. This restriction of the gradient allows much larger flexibility in the representation space, where $s_{ij} > 0$ and $s_{ii} < 1$. This extreme case showcases that removing gradient terms for low representation similarity regularizes dimensional collapse and motivates us to adapt the decoupled SimCLR loss similarly.

3.3. Subsampled Decoupled SimCLR

Method By selectively considering examples with high blockwise representations similarities, we aim to preempt the issue of dimensional collapse. For this, we fix a lower threshold value T to restrict the examples with similarity below and introduce for each module f^k:

$$\alpha^k_{\{i,l\}} \triangleq \mathbb{1}_{\mathrm{sim}(\boldsymbol{z}^k_i, \boldsymbol{z}^k_l) \geq T} \,. \tag{4}$$

Thus we obtain the loss for each positive pair $\{i, j\}$:

$$\ell^k_{i,j} = -\alpha^k_{\{i,j\}} \log \frac{\exp(\mathrm{sim}(\boldsymbol{z}^k_i, \boldsymbol{z}^k_j)/\tau)}{\sum_{l=1}^{2N} \mathbb{1}_{l \neq i} \alpha^k_{\{i,l\}} \exp(\mathrm{sim}(\boldsymbol{z}^k_i, \boldsymbol{z}^k_l)/\tau)} \,. \tag{5}$$

Toy example To understand the refinement of our method, we test it on the toy model of the linear framework of Jing et al. (2022), with standard normal noise data of dimension $D = 16$, augmented with standard normal noise with amplitude σ on the 8 last dimensions. We train our method following Eq. (5) with gradient descent. Compared to the gradient dynamic in Eq. (2), we use normalized representations. We report in Fig. 1a the singular values of the covariance matrix of the representations z. Standard SimCLR training produces collapsed dimensions, which disappear with our subsampling when increasing the threshold T as predicted.

4. Numerical experiments

Architecture We consider a ResNet-50 (He et al., 2016) base encoder, which we divide into 4, 8 or 16 decoupled blocks. Each local projector g^k is composed of a convolution and a multilayer perceptron. More details are given in the appendix.

Hyper-parameters and datasets We train the networks on three image classification datasets: CIFAR-10 (Krizhevsky et al.), Fashion-MNIST (Xiao et al., 2017) and STL-10 (Coates et al., 2011). Since Fashion-MNIST is an easier dataset than the others, we use a ResNet-18 model rather than a ResNet-50, and thus decouple only up to 8 blocks. Each block is trained using either the training objective Eq. (1) or (5). Following standard practice (Chakraborty et al., 2020), our model is trained with the Adam optimizer (Kingma & Ba, 2014) with a learning rate of 10^{-3} and weight decay of 10^{-6} for 1000 epochs, with batch size 256, and temperature is kept at the default $\tau = 0.5$. We choose the threshold T following the training accuracy in linear evaluation: $T = 0$ for CIFAR, $T = 0.3$ for Fashion-MNIST and $T = -0.4$ for STL-10.

4.1. Accuracy on image recognition tasks

Linear evaluation We evaluate the model train with a standard linear evaluation on the supervised image classification task. The model is frozen, and the representations at the end of the model are used to train a linear classifier. The layer is trained for 200 epochs with the cross-entropy loss, with the same optimizer and batch size as the self-supervised training. We use the STL-10 5k labeled training samples for training, like Löwe et al. (2019).

Classification results Tab. 1 reports testing accuracies on standard image datasets, comparing our method with the standard SimCLR loss, for splits in $K = 1, 4, 8$ and 16 blocks. As expected and previously noticed for supervised settings, the testing accuracy degrades as the number of splits increases. Introducing our data-sampling technique of Eq. (5) does not affect significantly our model if split in $K = 1$ or 4 blocks, since information loss is limited. The accuracy on STL-10 improves meaningfully only for $K = 16$. In the case of CIFAR-10, our sampling strategy allows us to improve the accuracy of $K = 16$ close to that of $K = 8$ with no subsampling, a significant improvement. We also show the high parallelization potential of our method, by providing the memory cost of our method as implemented, as well as the MACs value of the slowest block among the K, which is a lower bound MACs for a fully parallel model. We also confirm our findings for the easier Fashion-MNIST dataset in Tab. 2 for $T = 0.3$ on a ResNet-18. We find a similar improvement due to our subsampling method for $K = 8$, and a decrease for the end-to-end model.

4.2. Analysis of the internal representations.

Dimensional collapse We now investigate the extent of dimensional collapse in the representations generated by different methods. To do so, we consider the (average pooled) intermediate representations $(h^k_i)_i$ after training on CIFAR-10, from which we compute the covariance matrix and its

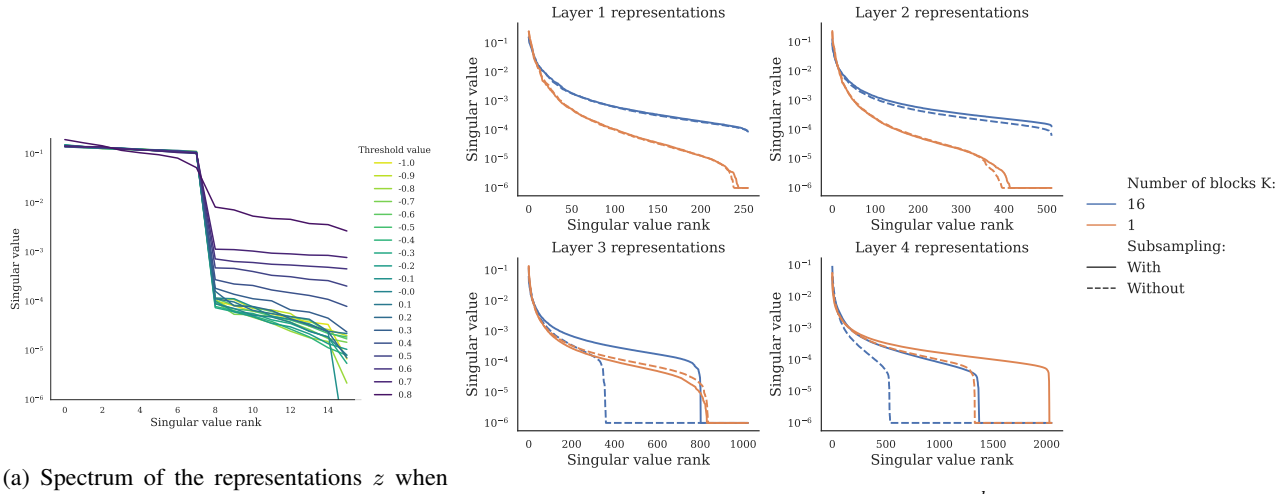

(a) Spectrum of the representations z when learning with our subsampled SimCLR strategy on the toy example with $\sigma = 1.5$. With no subsampling (yellow), the augmented features create collapsed dimensions at convergence, by contrast to the subsampling case (purple).

(b) Spectrum of the intermediate representations $(h_i^k)_i$ after each of the 4 ResNet layers on CIFAR-10; with models decoupled ($K = 16$) or not ($K = 1$) and trained with our without subsampling. With no subsampling, the spectra exhibit a fast decay at later layers, indicating a dimensionality collapse, while our subsampling results in a much higher features dimensionality even for $K = 1$.

Figure 1. Normalized spectrums of representations for the linear toy example and CIFAR-10.

singular value decomposition. We obtain the intrinsic dimensionality of the features, a linear proxy for their information content. Fig. 1b displays the spectrum for a ResNet-50 trained in various settings. The internal representations of the decoupled model trained on SimCLR suffers progressively from a dimensionality collapse, which is consistent with the findings of Wang et al. (2021) that found a drop in mutual information between the representations and both the labels and the input with depth.

However, we argue that our method prevents this dimensionality loss. We observe in the same figure the spectrum with and without subsampling. Despite no differences in the first layers, there is a significant increase in later layers both in the decoupled network and surprisingly in the End-to-End network. Notably, in the last layer, the dimensionality of the decoupled model matches the SimCLR-trained End-to-End model. Since the End-to-End model does not suffer from information loss, the dimensionality does not however improve its accuracy, compared to the decoupled model.

Linear probes To further study the effect of our subsampling, particularly relating to depth, we compute linear evaluation on the intermediate representations h^k with K linear probes. We report in Fig. 2 the accuracy of the linear probes after training for a model trained End-to-End with SimCLR, and a decoupled model ($K = 16$) trained with and without subsampling. We observe similar linear probes accuracy curves to those obtained in local supervised learning despite using the SimCLR loss, with progressive accuracy for the End-to-End model, and high accuracy in early blocks before plateauing for the decoupled network. The model trained with subsampling shows a similar curve, with a slightly increasing improvement through depth. Yet, we do not get a model closer to an End-to-End one; as we would observe a decrease of early layer accuracy.

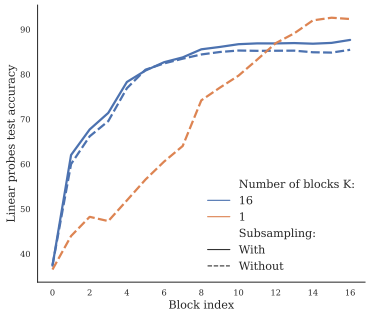

Figure 2. Linear separability on CIFAR-10 of intermediate representations h^k at various depth, estimated with linear probes. A model trained End-to-End will display slowly increasing test accuracy with depth, by contrast to a decoupled model which has much higher accuracy at low depth before plateauing. Our method indicates a consistent improvement compared to the original baseline.

Impact of the sampling during training We now study how sampling is affected during training. We report in Fig. 5 the ratio of positive and negative examples kept at each block during training, for a model trained on CIFAR-10 with $K = 16$ and $T = 0$. Surprisingly, almost all positive examples are kept during training despite the improvement provided by their removal. In comparison, as few as a

Table 1. Linear evaluation test accuracy results on CIFAR-10 and STL-10, after training on both SimCLR and our subsampling method (with mean and standard deviation over 5 runs for CIFAR-10). We also report the memory cost of local self-supervised learning and the maximum block MACs required among the K.

	Datasets	**CIFAR-10**			**STL-10**		
K	**Method**	**Accuracy**	**Max MACs**	**Memory**	**Accuracy**	**Max MACs**	**Memory**
1 (E2E)	SimCLR	**92.1** $\pm$ 0.2	1.31 G	13.5 GB	**87.6**	17.1 G	16.7 GB
	+ ours	91.4 $\pm$ 0.4			86.7		
4	SimCLR	**90.0** $\pm$ 0.1	349 M	8.7 GB	**84.3**	4.65 G	9.7 GB
	+ ours	89.9 $\pm$ 0.3			82.6		
8	SimCLR	87.5 $\pm$ 0.4	196 M	6.3 GB	**80.8**	2.63 G	7.0 GB
	+ ours	**88.4** $\pm$ 0.4			79.7		
16	SimCLR	85.9 $\pm$ 0.3	**123 M**	**5.6 GB**	77.8	**1.69 G**	**6.1 GB**
	+ ours	**87.1** $\pm$ 0.4			**78.8**		

Table 2. Linear evaluation test accuracy results on Fashion-MNIST of our method for $K = 1$ and 8 for $T = 0.3$ on a ResNet-18. We observe a similar improvement for this dataset. Results are shown in average for 5 runs.

K	**SimCLR**	**+ ours**
1 (E2E)	**91.3** $\pm$ **0.1**	90.3 $\pm$ 0.2
8	87.2 $\pm$ 0.3	**88.2** $\pm$ 0.3

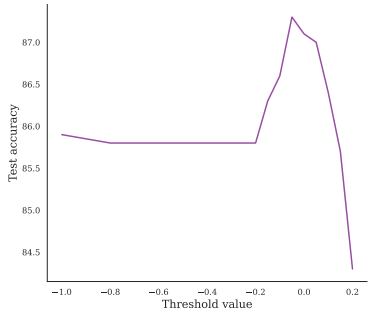

Figure 3. Test accuracy on CIFAR10 after training on SimCLR with $K = 16$ for varying threshold T. Accuracy peaks around $T = 0$, showing an equilibrium between the dimensionality increase and the removal of examples.

quarter of negative examples are kept in the last block at convergence, contradicting popular contrastive learning belief that more negative examples improve training. The ratio of negative examples kept decreases during training, which is not surprising as the model converges to have a negative alignment for negative examples. In both cases, the ratio kept decreases also with depth. With a difference of almost 10% between the first and last block, there are fewer negative examples to contrast with the positive ones in later blocks, which indicates a form of curriculum learning through depth.

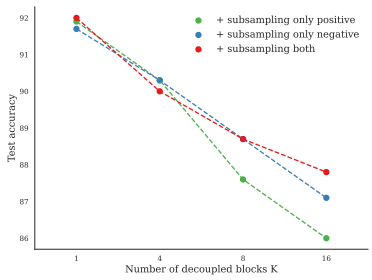

Figure 4. Test accuracy on CIFAR-10 depending on the number of decoupled blocks K after training on SimCLR with our subsampled method, by subsampling either positive or negative examples or both. Subsampling negative examples give the main improvement, but both are needed to reach the best accuracy.

Impact of the threshold value T We also study the accuracy of our model depending on the value of the threshold T, and find it to follow three piecewise linear curves. Below $T = -0.2$, accuracy is not improved as few examples are removed. There is a stark increase until approximately $T = 0$ before a decrease. This indicates an equilibrium between increasing dimensionality and removing too many examples. It is unclear why the accuracy peak is as sudden as it is.

Impact of the positive and negative examples To ensure that the removal of both positive and negative examples improves accuracy, we propose to train our method by subsampling only positive or negative examples. More precisely, in Eq. (5) we only add the term $\alpha^k_{\{i,j\}}$ to consider positive examples thresholding, or the denominator term $\alpha^k_{\{i,l\}}$ to consider negative examples thresholding. We report in Fig. 4 the accuracy of our method for varying K by subsampling

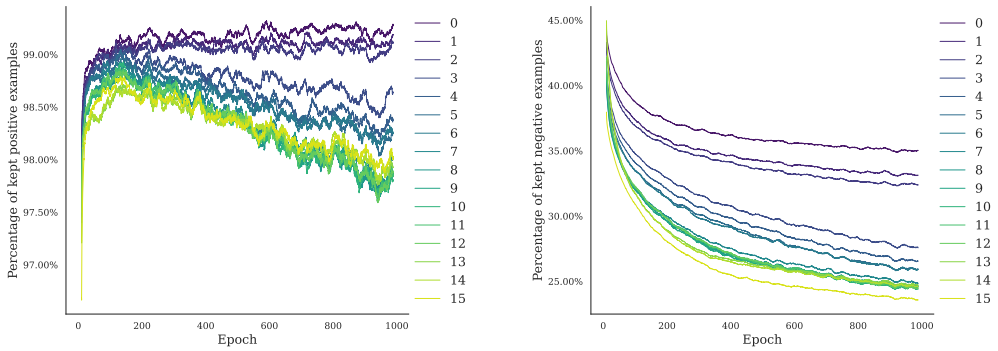

(a) Ratio of positive examples kept.

(b) Ratio of negative examples kept.

Figure 5. Ratio of positive and negative examples kept through training for each block. The model is trained with $K = 16, T = 0$ on CIFAR-10. Surprisingly, most positive examples are retained, indicating few outliers. The ratio of negative examples kept is much lower and decreases during training and with depth. Our method can be seen as a form of curriculum learning through depth.

either positive or negative examples or both. We report an improvement in both cases. Yet, thresholding all examples provides the best accuracy as K increases.

5. Conclusion

This paper investigated the training of DNNs with self-supervised local learning methods. We find that a dimensional collapse partially causes the drop in accuracy known in local learning with larger splits. By studying a linear model, we motivate a simple local feature similarity sampling method which improves on the original SimCLR loss. This method remedies this dimensional collapse, reducing the accuracy loss due to decoupling for models. However, decoupling still causes a significant accuracy gap, indicating other issues. We leave the generalization of our findings to non-contrastive self-supervised objectives for future work.

References

Belilovsky, E., Eickenberg, M., and Oyallon, E. Greedy layerwise learning can scale to imagenet. *Proceedings of the 36th International Conference on Machine Learning (ICML)*, 2019.

Belilovsky, E., Leconte, L., Caccia, L., Eickenberg, M., and Oyallon, E. Decoupled greedy learning of cnns for synchronous and asynchronous distributed learning. *arXiv preprint arXiv:2106.06401*, 2021.

Chakraborty, S., Gosthipaty, A. R., and Paul, S. G-simclr: Self-supervised contrastive learning with guided projection via pseudo labelling. In *2020 International Conference on Data Mining Workshops (ICDMW)*, pp. 912–916. IEEE, 2020.

Chen, T., Kornblith, S., Norouzi, M., and Hinton, G. A simple framework for contrastive learning of visual representations, 2020.

Coates, A., Lee, H., and Ng, A. Y. An analysis of single layer networks in unsupervised feature learning. *AISTATS*, 2011.

Gomez, A. N., Key, O., Perlin, K., Gou, S., Frosst, N., Dean, J., and Gal, Y. Interlocking backpropagation: Improving depthwise model-parallelism. *Journal of Machine Learning Research*, 23(171):1–28, 2022.

He, K., Zhang, X., Ren, S., and Sun, J. Deep residual learning for image recognition. In *Proceedings of the IEEE conference on computer vision and pattern recognition*, pp. 770–778, 2016.

He, K., Fan, H., Wu, Y., Xie, S., and Girshick, R. Momentum contrast for unsupervised visual representation learning, 2019. URL http://arxiv.org/abs/1911.05722. cite arxiv:1911.05722Comment: CVPR 2020 camera-ready. Code: https://github.com/facebookresearch/moco.

Illing, B., Ventura, J., Bellec, G., and Gerstner, W. Local plasticity rules can learn deep representations using self-supervised contrastive predictions, 2021.

Jaderberg, M., Czarnecki, W. M., Osindero, S., Vinyals, O., Graves, A., Silver, D., and Kavukcuoglu, K. Decoupled neural interfaces using synthetic gradients. In *International conference on machine learning*, pp. 1627–1635. PMLR, 2017.

Jing, L., Vincent, P., LeCun, Y., and Tian, Y. Understanding dimensional collapse in contrastive self-supervised learning, 2022.

Kingma, D. P. and Ba, J. Adam: A method for stochastic optimization. *arXiv preprint arXiv:1412.6980*, 2014.

Krizhevsky, A., Nair, V., and Hinton, G. Cifar-10 (canadian institute for advanced research). URL http://www.cs.toronto.edu/~kriz/cifar.html.

Löwe, S., O'Connor, P., and Veeling, B. S. Putting an end to end-to-end: Gradient-isolated learning of representations, 2019. URL https://arxiv.org/abs/1905.11786.

Nøkland, A. and Eidnes, L. H. Training neural networks with local error signals. In *International conference on machine learning*, pp. 4839–4850. PMLR, 2019.

Ren, M., Kornblith, S., Liao, R., and Hinton, G. Scaling forward gradient with local losses. *arXiv preprint arXiv:2210.03310*, 2022.

Robinson, J. D., Chuang, C., Sra, S., and Jegelka, S. Contrastive learning with hard negative samples. In *9th International Conference on Learning Representations, ICLR 2021, Virtual Event, Austria, May 3-7, 2021*. OpenReview.net, 2021. URL https://openreview.net/forum?id=CR1XOQ0UTh-.

Siddiqui, S. A., Krueger, D., LeCun, Y., and Deny, S. Blockwise self-supervised learning at scale, 2023.

Tabassum, A., Wahed, M., Eldardiry, H., and Lourentzou, I. Hard negative sampling strategies for contrastive representation learning, 2022.

Wang, Y., Ni, Z., Song, S., Yang, L., and Huang, G. Revisiting locally supervised learning: an alternative to end-to-end training. In *International Conference on Learning Representations (ICLR)*, 2021. URL https://openreview.net/forum?id=fAbkE6ant2.

Xiao, H., Rasul, K., and Vollgraf, R. Fashion-mnist: a novel image dataset for benchmarking machine learning algorithms, 2017. URL http://arxiv.org/abs/1708.07747. cite arxiv:1708.07747Comment: Dataset is freely available at https://github.com/zalandoresearch/fashion-mnist Benchmark is available at http://fashion-mnist.s3-website.eu-central-1.amazonaws.com/.

Xiong, Y., Ren, M., and Urtasun, R. Loco: Local contrastive representation learning. *Advances in neural information processing systems*, 33:11142–11153, 2020.

Appendix: Implementation details

The training was done on A100 GPUs, requiring 12 hours for a CIFAR-10 run on 1 GPU and 4 hours on 16 GPUs for STL10. The memory cost is the maximum memory allocated by CUDA, with cuDNN benchmarking turned off for consistency, on an A100 GPU with the same batch sizes as for the training.

Architecture details The model we study is a ResNet-50, composed of a convolutional layer, a BatchNorm layer followed by a ReLU activation and a max pooling layer, then 16 Bottleneck blocks, a final global average pooling and a fully connected layer; following Pytorch official implementation at https://github.com/pytorch/vision/blob/main/torchvision/models/resnet.py.

Since the datasets we consider have lower image sizes than the ImageNet dataset for which the ResNet model was initially designed for, we propose different first layers before the bottleneck layers, as standard. For STL-10, CIFAR-10 and Fashion-MNIST datasets, we remove the max pooling layers. For STL-10, the convolution layer is the same as standard, except for a slight reduction of kernel size from 7 to 5. For the other smaller datasets, the convolution layer has a kernel size of 3, and stride and padding of 1.

Table 3. Decoupling points of our ResNet-50 architectures depending on the number of blocks K. The network is composed of 4 main Layers, each composed of $3, 4, 6$ and 2 Bottleneck blocks respectively. At each decoupling point, the local training loss is computed and backpropagated, and the following representations pass through a StopGrad operator to prevent gradients between blocks.

K	Decoupling points (after Layer i and Bottleneck j)
4	(2, 1), ((3, 1), (3, 5))
8	(1, 2), ((2, 1), (2, 3)), ((3, 1), (3, 3), (3, 5)), (4, 1)
16	After each Bottleneck

Split details Our model is decoupled at several 'decoupling points' where gradient information is stopped. For $K = 4, 8$ the split is adjusted to maintain an equal number of bottlenecks in each block, leading for $K = 16$ to split after the bottleneck of each block. To be more precise on the location of these decoupling points, we refer to Table 3, where we localize them with the layer (out of 4) and bottleneck numbers starting from 1.

Each local projector g^k is composed of: a 3×3 convolutional layer (with stride 2 and the same number of channels as the representation), a batch normalization and ReLU layer, a global average pooling, then a fully connected layer, a ReLU, and a final fully connected layer with output dimension 128. Note also that the auxiliary projector networks

used in our methods are used at every decoupling point before the local loss, but not for the final layer, which uses the classical 2-layer MLP projection head.

Augmentation details Images are augmented following the simple augmentation procedure proposed by SimCLR without Gaussian Blur: a Random Resized Crop to the necessary image size, a random horizontal flip (with probability 0.5), a random color jitter (with probability 0.8 and brightness contrast and saturation parameters equal set to 0.4 and hue to 0.1) and random color dropping (setting to grayscale, with probability 0.2). Test images are not augmented.